

UnderOak Observer

Issue 3 · January - March 2012

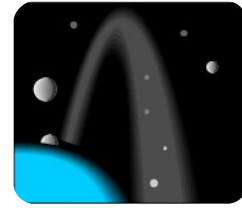
**Losmandy G11 Tune-up:
Ovision Worm-Gear Upgrade**

Lightcurve Analysis of 31 Euphrosyne

Mining the Kepler Mission Database

Photometry With HyperStar 3 Optics

Lightcurve Analysis of the Minor Planet 31 Euphrosyne



Abstract

Clear filter CCD images of 31 Euphrosyne were acquired on three nights between 25Nov2011 and 02Dec2011 and then used to produce lightcurves and determine the synodic period (5.53 hr) for this main belt asteroid.

Introduction

Observed in 1854 by the American astronomer James Ferguson, this was the first documented discovery of an asteroid from a North American location (Naval Observatory in Washington D.C.). Although not a household name like Ceres or Vesta, the minor planet 31 Euphrosyne (255.9 km) is considered the fifth most massive minor planet (Baer et al 2008). Despite its high rank in size and mass, chronologically 31 Euphrosyne was the 14th such object to be detected largely owing to its dark low albedo surface commonly attributed to C-type asteroids. In addition, its orbit around the Sun is highly inclined and eccentric (Figure 1) relative to Earth's ecliptic, which is atypical for most main-belt asteroids.

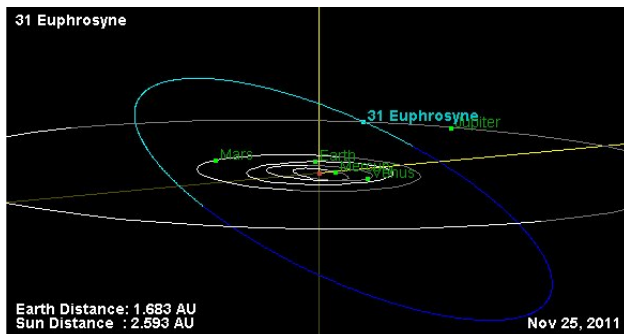


Figure 1. Orbit Diagram for 31 Euphrosyne Produced Using Orbit Viewer Applet Available at the JPL Small-Body Database

The first documented light curves for 31 Euphrosyne were published by Schober et al in 1980. Other published studies conducted since then include Lincando et al (1990), Pilcher and Jardine (2009), Oey (2010), as well as investigations to unravel the three dimensional morphology and spin axis (McCoyne

et al 1985, Lincando et al 1994; Kryszyńska et al, 1996 and Torppa et al 2008). Despite efforts to date, the axial tilt (obliquity) of this asteroid is still not well defined (Torppa et al 2008). To this end the lightcurve data generated at UnderOak Observatory may prove useful in improving a shape and spin solution for 31 Euphrosyne.

Results and Discussion

For this study a 0.2-m Schmidt-Cassegrain telescope (f/10) was coupled with a thermoelectrically cooled (-10°C) SBIG ST-402ME CCD camera mounted with a motorized focuser. Images captured by this optical train produce a 7.2×10.7 arcmin field-of-view with a resolution of 0.84 arcsec/pix. To ensure accurate timings, the computer clock was automatically updated (Dimension 4; <http://www.thinkman.com/dimension4/>) via the USNO server before every run. Clear filter images were continually captured every 45 seconds during each session. Raw lights, darks and flats acquired using CCDSoft 5 were calibrated and registered with AIP4WIN (Berry and Burnell 2008). MPO Canopus (Warner 2010) was used to generate light curves by differential aperture photometry by including at least two non varying comparison stars captured each evening. A total of 943 light curve values were acquired over 7 days; data were not reduced to standard magnitudes but were light time corrected.

UT Date (2011)	No. Obs	Phase Angle	L_{PAB}	B_{PAB}	%Phase Coverage
Nov 25	128	10.6	40.5	8.9	29.5
Nov 26	408	11.0	40.5	9.0	103.4
Dec 2	405	13.2	40.7	9.7	98.3

MPO Canopus yielded a period solution (Figure 2) for the folded data sets using Fourier analysis (Harris 1989). The synodic period (5.53 hr) was in very good agreement with rotational periods for this asteroid published by others and that reported by the “Small-Body Database Browser” at the JPL Solar System Dynamics website. In addition, the light curve amplitude (~0.12 mag) was within the range

(0.07-0.2 mag) observed in previous investigations. Relevant aspect parameters for 31 Euphrosyne taken at the mid-point from each session are tabulated below.

Acknowledgement

The SAO/NASA Astrophysics Data System (http://adsabs.harvard.edu/abstract_service.html) was used to conduct literature searches in support of this study.

References

Baer, J., Milani, A., Chesley, S. and Matson, R.D. (2008), "An Observational Error Model, and Application to Asteroid Mass Determination, Bull.American Astron. Society, 40, 493.
 Berry, R. and Burnell, J. (2008), AIP4WIN version 2.3.1, Willmann-Bell, Inc, Richmond, VA.
 Harris, A.W., Young, J.W., Bowell, E., Martin, L. J., Millis, R. L., Poutanen, M., Scaltriti, F., Zappala, V., Schober, H. J., Debehogne, H, and Zeigler, K. (1989), "Photoelectric Observations of Asteroids 3, 24, 60, 261, and 863." Icarus 77, 171-186.
 JPL Solar System Dynamics website (<http://ssd.jpl.nasa.gov/sbdb.cgi>)
 Kryszczyńska, A., Colas, F. Berthier, J., Michalowski, T. and Pych, W. (1996), "CCD Photometry of Seven Asteroids: New Spin Axis and Shape Determinations", Icarus, 124, 134

Licandro, J., Gallardo, T. and Tancredi, G. (1990), "Photometric Observations of Asteroids 31 Euphrosyne, 118 Peito, 13 Egeria, 196 Philomena and 471 Papagena", Revista Mexicana de Astronomia y Astrofisica, 21, 590
 Licandro, J., Gallardo, T. and Tancredi, G. (1994), "Lightcurves and Pole Determinations for Asteroids 31 Euphrosyne, 196 Philomena and 471 Papagena", Revista Mexicana de Astronomia y Astrofisica, 28, 91
 McCheyne, R.S., Eaton, N., and Meadows, A.J. (1985), "Visible and Near-Infrared Lightcurves of Eight Asteroids", Icarus, 61, 443
 Oey, J. (2010), "Light Curve Analysis of Asteroids from Leura and Kingsgrove Observatory in the First Half of 2009", Minor Planet Bulletin, 37, 135
 Pilcher, F. and Jardine, D. (2009), "Period Determinations for 31 Euphrosyne, 35 Leukothea, 56 Melete, 137 Meliboea, 155 Scylla and 264 Libussa", Minor Planet Bulletin, 36, 52
 Schober, H.J., Scaltriti, F., Zappala, V. and Harris, A.W. (1980), "The Remaining Large Minor Planets with Unknown Rotational Properties – 31 Euphrosyne and 65 Cybele", Astron. & Astrophys., 91, 1
 Torppa, J., Hentunen, V.-P., Pääkkönen, P., Kehusmaa, P. and Muinonen, K. (2008), "Asteroid Shape and Spin Statistics from Convex Models", Icarus, 198, 91
 Warner, B.D. (2010), MPO Canopus version 10.3.0.2. Bdw Publishing, Colorado Springs, CO.

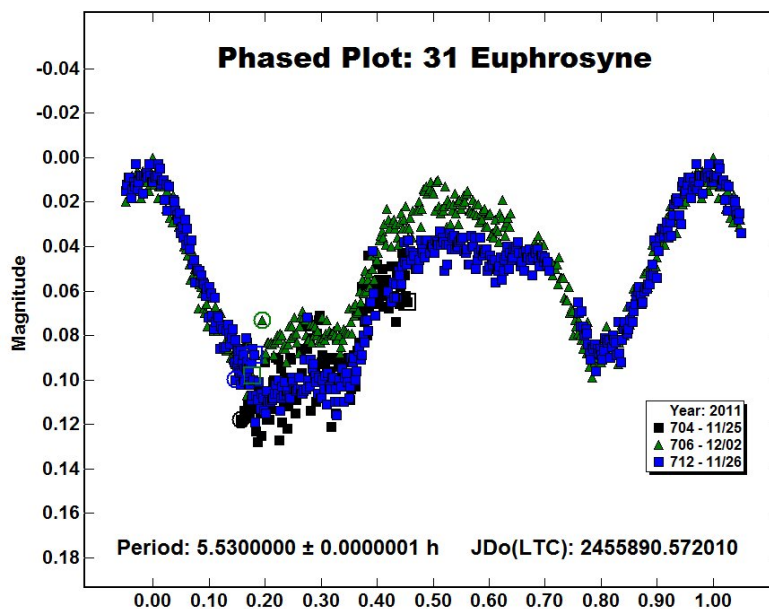


Figure 2
 Folded light curves (phase vs relative flux) from the 2011 photometric campaign of 31 Euphrosyne

Mining the Kepler Mission Database - Part I

The Kepler space satellite is best known in the lay press for reporting the possible detection of Earth-like worlds circling far-off suns, yet by comparison to this primary objective, the Kepler mission will most assuredly lead to the discovery of far more traditionally defined intrinsic or extrinsic variable stars. The Kepler spacecraft employs a 0.95m Schmidt-design telescope and a 42 CCD array which continuously monitors ~156,000 stars during its heliocentric Earth-trailing orbit. The 105 deg² field-of-view is centered (RA=19^h22^m40^s and decl.=44°30'00") at the Cygnus-Lyra border approximately between Deneb and Vega.

PlanetHunters.org Portal

Other than press articles featured in Astronomy and Sky&Telescope magazines, my first direct exposure to the raw data being captured by Kepler Mission was through PlanetHunters.org, a Zooniverse (<https://login.zooniverse.org/>) portal specifically established to involve "Citizen Scientists" in the search for exoplanets.

Entry into PlanetHunters.org or any of the other Zooniverse projects requires one to register and open an account. A tutorial is available which walks the uninitiated investigator through the process of identifying the light curve signature of an exoplanet. The light curve for SPH10009439 (Figure 1) is a fairly uncomplicated example of the effect that a potential exoplanet has on the light signal as it transits in front of its host star. This can be seen as the two very sharp downward excursions from the background noise, in this case separated by 12.23 days, the apparent planetary orbital period. It is important to note the y-axis scale which measures the change in star brightness. In this example it only ranges between 1.009 and 1.005, with the exoplanet signal representing a very small decrease (~0.002) in light during transit. This miniscule difference is typical of many other exoplanet discoveries and is testimony to the extraordinary sensitivity of the Kepler CCD detection system. As a side note, each time an interesting light

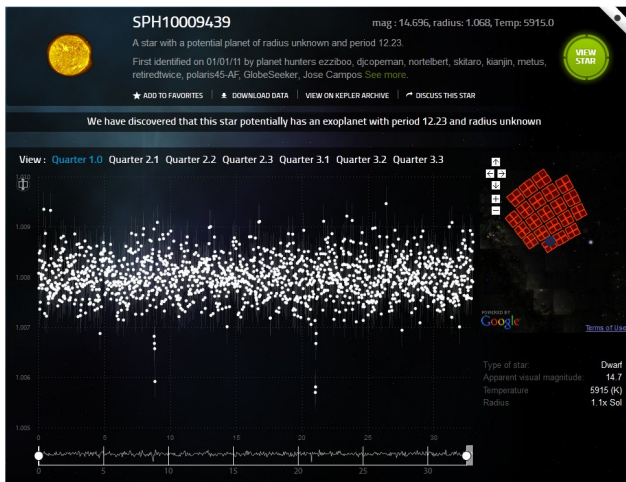


Figure 1. Lightcurve of Potential Exo-planet Orbiting SPH10009439

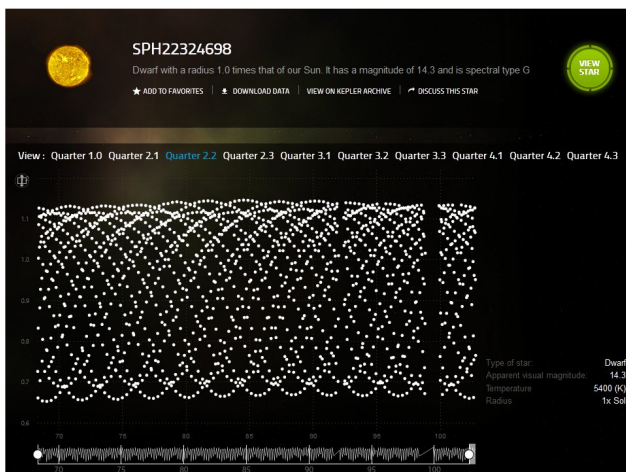


Figure 2. Lightcurve from Eclipsing Binary System SPH22324698 Captured by Kepler During 2010

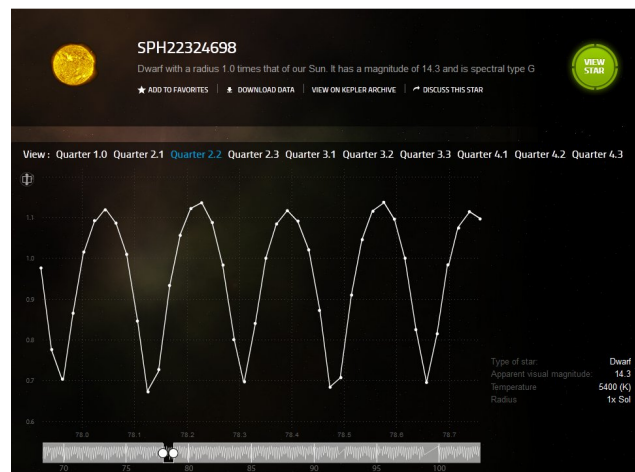


Figure 3. Lightcurve of Typical W UMa Overcontact Binary System

	A	B	C	D	E	F	G	H	I	J	K	L	M	N
1	dec	eff_temp	h_mag	j_mag	k_mag	kepler_id	kepler_mag	Simulation/Planet Candidate	log_g	ra	spec_type	star_type	stellar_rad	zooviverse_id
2		0	5400	12.615	12.976	12.538	kplr009389122	14.313	Simulation	4.446	0 G	Dwarf	1.001	SPH22324698
5	Quarter	time (days)	brightness	error in brightness										
6	2.2	0.017265	0.726014197	0.000196672										
7	2.2	0.037698	0.660890698	0.000196023										
8	2.2	0.058132	0.832177699	0.000195375										
9	2.2	0.078566	1.00368464	0.000194376										
10	2.2	0.098999	1.08598774	0.000193497										

Figure 4. Top Rows of Spreadsheet Produced From Downloading Lightcurve file from PlanetHunter.org Website

KEPLER

MAST STScI Tools Mission Search Tutorial Site Search

Kepler Home About Kepler Getting Started Registration Kepler Data Search Kepler Target Search FFI Search

Archive Status **Kepler Data Search & Retrieval** (Help) Field Descriptions

Standard Form File Upload Form

Search Reset Clear Form

Target Name Resolver Radius (arcmin)

Right Ascension Declination Equinox

Kepler ID Investigation ID 2Mass ID

KEP Mag Target Type Release Date

Teff Log_G Condition Flag

User-specified field 1 Field Descriptions User-specified field 2 Field Descriptions

User-specified field 3 Field Descriptions User-specified field 4 Field Descriptions

Output Columns Sort By:

ang_sep () Reverse

KeplerID Reverse

null Reverse

Output Coords: Sexagesimal Degrees Hours

Output Format HTML_Table

Show Query Make Rows Distinct

Maximum Records: 1001

Records per Page: 100

Search Reset Clear Form

Top of Page Copyright Email Us Printer Friendly page Contacts Last Modified: Jan 10, 2011 15:46

Figure 5. Kepler Mission Data Search & Retrieval Form

curve is encountered it can be saved as a “favorite” and thereafter downloaded at your convenience. The file structure is a comma separated value format (*.csv) so that it can be easily imported into a spreadsheet program.

As rewarding as it was to search for the home base of potential extraterrestrials, I was equally intrigued by the myriad of geometric light curve designs weaved by the periodic pulsation of stars or eclipsing events from binary stars. A great example of this can be seen for SPH22324698 in Figure 2. Let’s dig a little deeper and unravel the mystery behind this light curve mosaic. By adjusting the x-axis (Barycentric Julian Date; BJD) to a shorter time span, connected data points begin to produce a light curve outline typical of an eclipsing binary (Figure 3). More specifically, this system would appear to be a W UMA type over-contact binary based upon its signature shape. The spectral type of this variable system is estimated by the Kepler team to be a G7-G8 dwarf with an effective temperature (Teff) around 5400 K which is slightly cooler than our own sun (5800 K).

The header (first two lines) from the downloaded spreadsheet file (SPH223224698.csv) contains important information about the system which can potentially be used to build a model to explain the associated light curve behavior and refine the physical characteristics of each variable star (Figure 4). The light curve data are divided into quarters and time (days) during which the data were collected along with the brightness and error term for each time point. These files can be used to reconstruct a light curve by inserting a scatter chart within Excel or its free equivalent LibreOffice Calc.

More rigorously (as will be discussed further on), the definitive raw data is maintained as a fits-type file and can be accessed through the Kepler Archives (http://archive.stsci.edu/kepler/manuals/archive_manual.pdf). Assuming that you encountered an interesting target at PlanetHunters.org, the following procedure proved to be the most straightforward. The official Kepler designation for each Zooniverse object (SPH prefixed file) is embedded in the *.csv file header which in the example above is “kplr009389122”. The Kepler Data Search & Retrieval Form (Figure 5)

Kepler Data Search Results

number of rows returned = 10

Click on top column headers to sort the table on the column contents.
Click on bottom column headers for more information about the data in that column.
Click on Ref entries to display list of published papers.

Mark	Kepler ID	Dataset Name	Quarter	RA (J2000)	Dec (J2000)	Actual Start Time	R Mag	J Mag	KEP Mag	2MASS ID	Teff	Log G	Metallicity	E(B-V)	Radius
<input type="checkbox"/>	9389122	KPLR009389122-2009166043257	1	18 56 20.01	+45 56 48.7	2009-05-13 00:15:49	14.213	12.976	14.313	18562000+4556486	5400	4.446	0.101	0.092	1.001
<input checked="" type="checkbox"/>	9389122	KPLR009389122-2009259160929	2	18 56 20.01	+45 56 48.7	2009-06-20 00:25:09	14.213	12.976	14.313	18562000+4556486	5400	4.446	0.101	0.092	1.001
<input type="checkbox"/>	9389122	KPLR009389122-2009350155506	3	18 56 20.01	+45 56 48.7	2009-09-18 17:19:58	14.213	12.976	14.313	18562000+4556486	5400	4.446	0.101	0.092	1.001
<input type="checkbox"/>	9389122	KPLR009389122-2010078095331	4	18 56 20.01	+45 56 48.7	2009-12-19 21:03:56	14.213	12.976	14.313	18562000+4556486	5400	4.446	0.101	0.092	1.001
<input type="checkbox"/>	9389122	KPLR009389122-2010174085026	5	18 56 20.01	+45 56 48.7	2010-03-20 23:47:15	14.213	12.976	14.313	18562000+4556486	5400	4.446	0.101	0.092	1.001
<input type="checkbox"/>	9389122	KPLR009389122-2010265121752	6	18 56 20.01	+45 56 48.7	2010-06-24 22:44:09	14.213	12.976	14.313	18562000+4556486	5400	4.446	0.101	0.092	1.001
<input checked="" type="checkbox"/>	9389122	KPLR009389122-2010355172524	7	18 56 20.01	+45 56 48.7	2010-09-23 16:08:24	14.213	12.976	14.313	18562000+4556486	5400	4.446	0.101	0.092	1.001
<input checked="" type="checkbox"/>	9389122	KPLR009389122-2011073133259	8	18 56 20.01	+45 56 48.7	2011-01-06 20:45:08	14.213	12.976	14.313	18562000+4556486	5400	4.446	0.101	0.092	1.001
<input checked="" type="checkbox"/>	9389122	KPLR009389122-2011177032512	9	18 56 20.01	+45 56 48.7	2011-03-21 00:24:25	14.213	12.976	14.313	18562000+4556486	5400	4.446	0.101	0.092	1.001
<input checked="" type="checkbox"/>	9389122	KPLR009389122-2011271113734	10	18 56 20.01	+45 56 48.7	2011-06-27 08:14:32	14.213	12.976	14.313	18562000+4556486	5400	4.446	0.101	0.092	1.001

Figure 6. Kepler Search Result Listing of kplr009389122 Data Available by Quarter

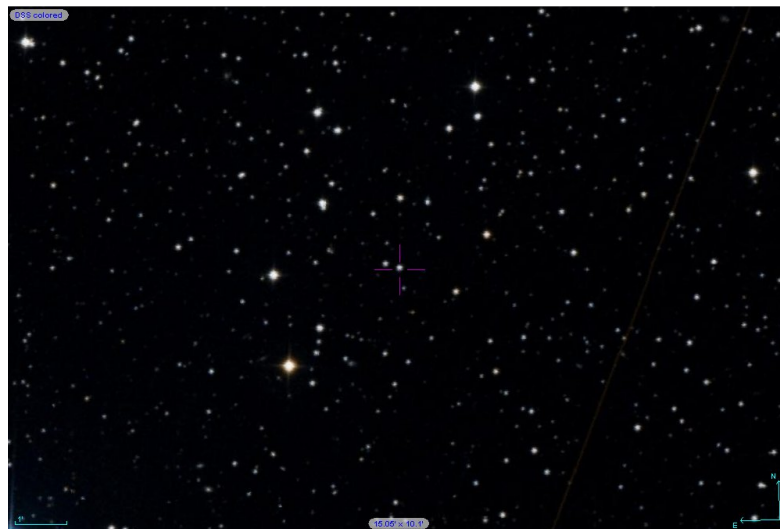


Figure 7. Image Produced by Aladin Showing that kplr009389122 is not Contaminated by any Significant Unresolved Star

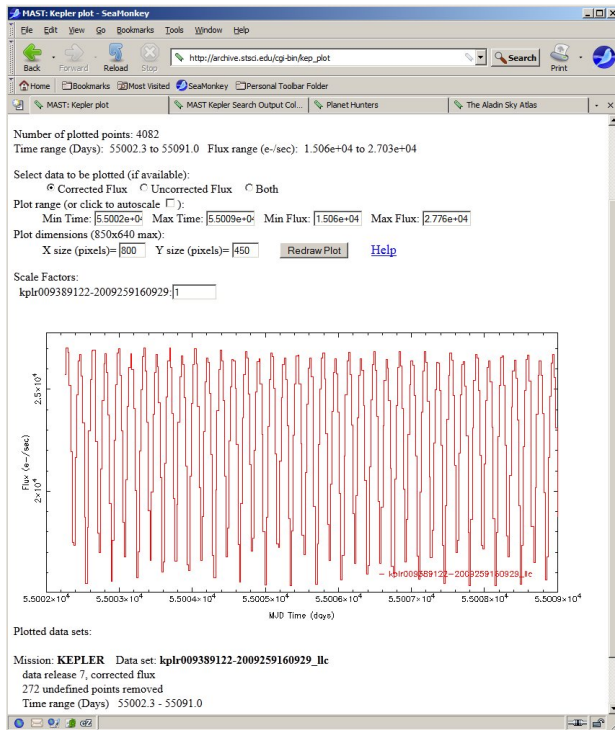


Figure 8. Plotting Option Provided Within Kepler Data Search Tool Which Can Quickly Reproduce a Lightcurve

provides the user with a customizable query to the database (http://archive.stsci.edu/kepler/data_search/search.php). All that is necessary to begin a search is the Kepler ID number without the “kplr” prefix. A few fields were deselected to simplify the HTML output shown below (Figure 6). The first order of business is to verify that the target of interest is not contaminated by an unresolved star which could potentially complicate interpretation of the light curve. Aladin (<http://aladin.u-strasbg.fr/aladin.gml>) allows the user to visualize digitized star charts and superimpose entries from a large number of astronomical catalogs. Following entry of the RA and Dec coordinates for kplr009389122, Aladin reveals that this Kepler target (aka 2MASS 18562000+4556486) appears to be a single object and is untouched by any obvious nearby star (Figure 7). A quick graphical inspection can be accomplished by selecting any dataset, pressing the “Plot marked light curves” button and then adjusting the plot range for corrected flux when the plotted results appear (Figure 8). Now satisfied that the proper dataset(s) have been identified, a return to the Kepler Search Results page will find another option which is “Submit marked data for retrieval from STDADS”. We’ll need to step back for a moment since in order to submit a request for data, a MAST

Datasets Marked for Retrieval

[Archive Status](#)

NEW [Important Downtime Message](#) **NEW**

2 datasets (2 public, 0 proprietary) marked.

Submit marked data for retrieval from STDADS

Mark all Unmark all Mark proprietary Unmark proprietary Mark public Unmark public

Row	Mark	Dataset	Class	Release	Archived	Row
1	<input checked="" type="checkbox"/>	KPLR009389122-2009259160929	CLC	2011-02-02 06:00:00	2011-07-17 19:21:51	1
2	<input checked="" type="checkbox"/>	KPLR009389122-2009259160929	TPL	2011-02-02 06:00:00	2011-02-08 15:22:49	2

Submit marked data for retrieval from STDADS

Mark all Unmark all Mark proprietary Unmark proprietary Mark public Unmark public

Mon Jan 23 11:42:59 2012
archive@stsci.edu

Copyright © 2012 AURA, Inc.
 All Rights Reserved.

Figure 9. Kplr009389122 Public Datasets from 2Q Selected for Retrieval

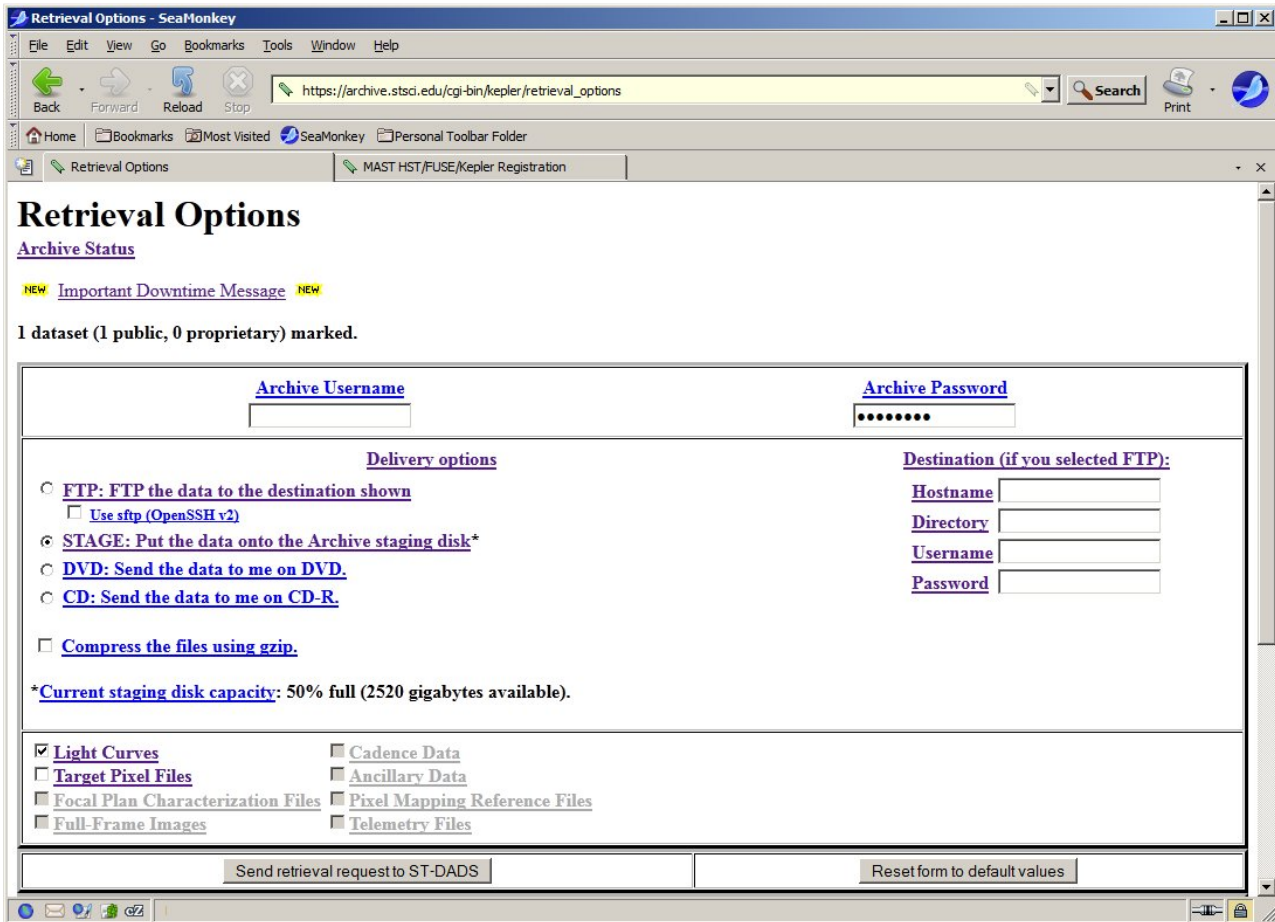


Figure 10. Archive Retrieval Options Form in Which Light Curve Data (but not Target Pixel Files) are to be Sent to Archive Staging Disk

(Multimission Archive at STSci) users account must be obtained. At the top of the Kepler Data Search & Retrieval Form (Figure 5) you'll find a "Registration" button which leads to all the information necessary to establish an account.

Assuming for the moment that you have already registered, then we can move on to the next step. For any given target, archive users can retrieve the raw and calibrated pixel values from the target pixel files (TPL) or the integrated flux values contained in the light curves (CLC).

For simplicity's sake in this exercise, let's narrow the retrieval options to only the CLC class datasets. After entering your Archive Username and Archive Password proceed by pressing the "Submit marked data for retrieval from STDADS" button one more time to reveal the last form (Figure 10). You can either have the data FTP'd to a specific destination or have it placed onto the Archive staging disk for pickup. Either option gets performed quite efficiently producing an e mail alert that the job request has been received followed quickly by a note that the delivery status is successful. My preference is to transfer data to the remote archive staging disk and retrieve files using FileZilla (<http://filezilla-project.org/>), a free cross platform FTP, FTPS and SFTP client with an intuitive graphical user interface. Once the selected files reside on your computer, light curve investigations can begin in earnest. You should also note that most files (*_*_lrc.fits) are derived from long cadence (29.4 min) bins, however, there are some special cases (*_*_slc.fits) in which a much shorter cadence (59 sec) sampling rate was used to improve resolution.

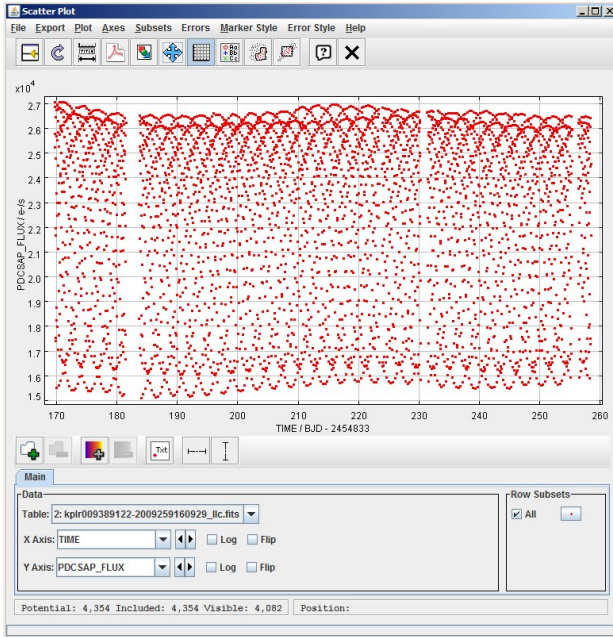


Figure 11. TOPCAT Output Scatter-Plot of kplr009389122 2nd Quarter Data

Much of what will be discussed from this point forward is focused on kplr009389122; however, the same basic principles apply to any stellar target with a periodic change in brightness. Each Kepler fits file contains all the information necessary to produce a light curve over the prescribed period of time, but is not readable by image processing programs (eg AIP4Win, MaxDL 5) that are typically used by amateur astronomers. To fulfill this need, there are two applications freely available at the Kepler website (<http://keplergo.arc.nasa.gov/DataAnalysisTools.shtml>) which allows thorough examination of the imbedded data. These include "fv" which is best suited to review the target pixel data to determine whether there is contaminating light from an unresolved light source, and TOPCAT which provides a more user-friendly GUI interface to retrieve and display tabulated light curve data for each Kepler object. A typical scatter-plot output from TOPCAT is shown (Figure 11) for the full set of 2nd Quarter data collected from kplr009389122. A tabulated presentation of data (Figure 12) can be displayed which includes all parameters or a customized selection with fewer data fields. These in turn can be

	TIME	TIMECORR	CADENCENO	SAP_FLUX	SAP_FLUX_ERR	SAP_BKG	SAP_BKG_ERR	PDCSAP_FLUX	PDCSAP_FLUX_ERR	SAP_QUALITY
1	169.51939	0.001915	2965	17843.	4.16371					256
2	169.53982	0.001915	2966	18551.	4.18455					256
3	169.56026	0.001916	2967	22926.	4.20529					256
4	169.58069	0.001916	2968	25799.	4.22593					256
5	169.60113	0.001916	2969	27324.	4.24646					256
6	169.62156	0.001917	2970	27467.	4.2669					256
7	169.64199	0.001917	2971	26235.	4.28724					256
8	169.66243	0.001918	2972	23712.	4.30749					256
9	169.68286	0.001918	2973	18835.	4.32764					256
10	169.7033	0.001918	2974	16225.	4.34769					256
11	169.72373	0.001919	2975	19643.	4.36766					256
12		0.	2976							1
13	169.7646	0.001919	2977	26358.	4.40731			25736.	4.17098	0
14	169.78503	0.00192	2978	27635.	4.42701			27018.	4.26414	0
15	169.80547	0.00192	2979	27453.	4.44662			26835.	4.29397	0
16	169.8259	0.001921	2980	25810.	4.46614			25201.	4.34112	0
17	169.84633	0.001921	2981	22553.	4.48558			21936.	4.3689	0
18	169.86677	0.001921	2982	18098.	4.50493			17484.	4.38684	0
19	169.8872	0.001922	2983	17970.	4.5242			17358.	4.42915	0
20	169.90764	0.001922	2984	22259.	4.54339			21646.	4.45056	0
21	169.92807	0.001922	2985	25362.	4.5625			24747.	4.47628	0
22	169.9485	0.001923	2986	27015.	4.58152			26404.	4.48707	0
23	169.96894	0.001923	2987	27335.	4.60047			26720.	4.52107	0
24	169.98937	0.001924	2988	26252.	4.61935			25643.	4.53693	0
25	170.00981	0.001924	2989	23957.	4.63814			23346.	4.55809	0
26	170.03024	0.001924	2990	19337.	4.64919			18729.	4.56777	0
27	170.05067	0.001925	2991	16091.	4.66022			15484.	4.57832	0
28	170.07111	0.001925	2992	18829.	4.67122			18216.	4.60021	0
29	170.09154	0.001925	2993	23576.	4.6822			22967.	4.60845	0
30	170.11198	0.001926	2994	26086.	4.69315			25480.	4.62867	0
31	170.13241	0.001926	2995	27504.	4.70407			26901.	4.63934	0
32	170.15284	0.001927	2996	27526.	4.71497			26925.	4.65647	0
33	170.17328	0.001927	2997							32
34	170.19371	0.001927	2998	23051.	4.7367			22449.	4.65554	0
35	170.21415	0.001928	2999	18546.	4.74752			17947.	4.68026	0
36	170.23458	0.001928	3000	17607.	4.75832			17004.	4.70014	0
37	170.25501	0.001928	3001	21703.	4.76909			21103.	4.70363	0
38	170.27545	0.001929	3002	25055.	4.77985			24456.	4.70696	0

Figure 12. TOPCAT Tabulated Lightcurve Data from kplr009389122

saved to a *.csv file for import into a spreadsheet whereafter time vs brightness matchings can be further processed using software (eg Peranso, Periodo4 or Famias) designed to determine whether the dataset exhibits regular periodicity. It is not uncommon to find null entries in the tabulated data so that these need to be culled out before saving in a file format suitable for period analysis by any of the three aforementioned programs. With TOPCAT, the easiest way is to “sort down” on PDCSAP_FLUX, highlight all rows containing null data, define a new subset containing all unselected rows and then save the new subset. Peranso (<http://www.peranso.com/>) is a commercial PC application well worth the modest investment (\$45) whereas both Periodo4 (<http://www.univie.ac.at/tops/Periodo4/>) and Famias (<http://www.ster.kuleuven.be/~zima/famias/>) are freeware.

VStar (<http://www.citizensky.org/teams/vstar-software-development>), is a Java-based multi-platform visualization and period analysis application uniquely capable of reading the latest kplr*-*.*lc.fits files directly. VStar v2.13 which contains this functionality was in the midst of final testing while preparing this document and should have been released by the time this issue of the “UnderOak Observer” hits the web. The same dataset (kplr009389122) previously examined with TOPCAT is shown in Figure 13 when loaded into VStar. After highlighting a small segment of the light curve data, a single cycle can be visualized in order to obtain an estimate of the variable period (Figure 14). In this case, the period of time between the deepest two minimums is somewhat less than 0.4 days (the connected lines have been added for clarity using PhotoShop). The present version of VStar is capable of performing both date compensated discrete Fourier transform (DC DFT) or weighted wavelet z-transform (WWZ). Those interested in learning more about time-series analyses are encouraged to read a paper by Templeton (2004) which describes DC DFT, WWZ and other approaches to investigating time-varying systems. A DC DFT standard scan on kplr009389122 produces a power spectrum (Figure 15) which reveals at least three significant time-series events that occur at frequencies of 5.714464, 11.428928 and 2.857232 d⁻¹ (or with periods of 0.1749945, 0.0874973 and 0.3499891 d). A folded lightcurve using an initial period of 0.349989 d from the "Top Hits" panel is displayed in Figure 16. This can be refined by narrowing the Fourier analysis between 2.7 and 3.0 d⁻¹, and increasing the resolution to 0.00001. A new power spectrum (Figure 17) yields an improved fit (Figure 18) when the orbital frequency is adjusted to 2.85760 d⁻¹ (0.349944 d). This value agrees favorably with recently published (Prša et al 2011) results for this spectral class G over-contact eclipsing binary system which is also posted (<http://keplerebs.villanova.edu/>). The linear ephemeris for this system is defined by the following equation: $\text{Min I} = \text{BJD } 2,454,964.907967 + 0.349950 E$ based upon the first 120 days of observation (Prša et al 2011).

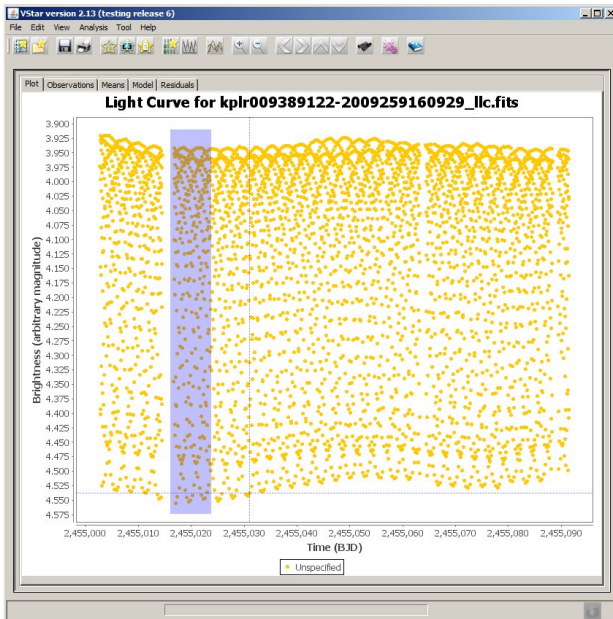


Figure 13. VStar Plot of All 2nd Quarter Lightcurve Data for kplr009389122

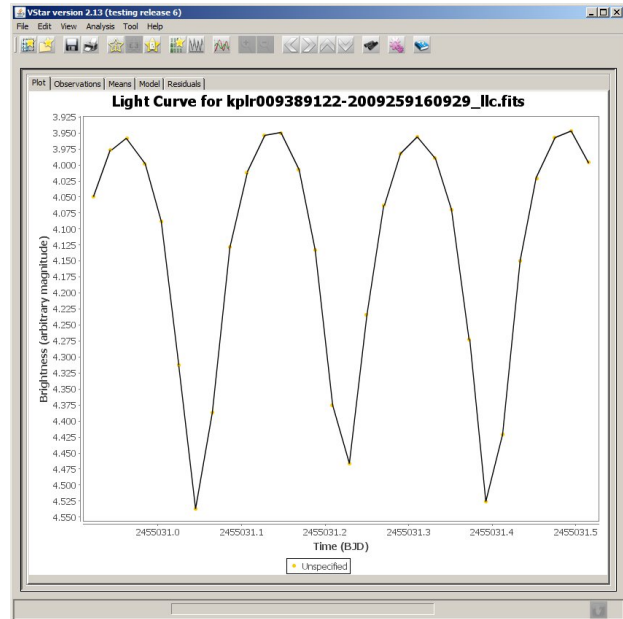


Figure 14. VStar Plot kplr009389122 Between BJD 2455031.0 and 2455031.5 Showing a 1.5 Period Cycle of Lightcurve Data

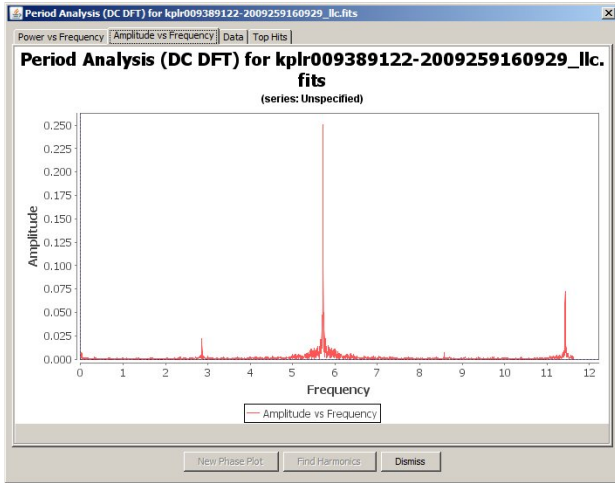


Figure 15. DC DFT Standard Scan of kplr009389122 2nd Quarter Lightcurve Data (Above)

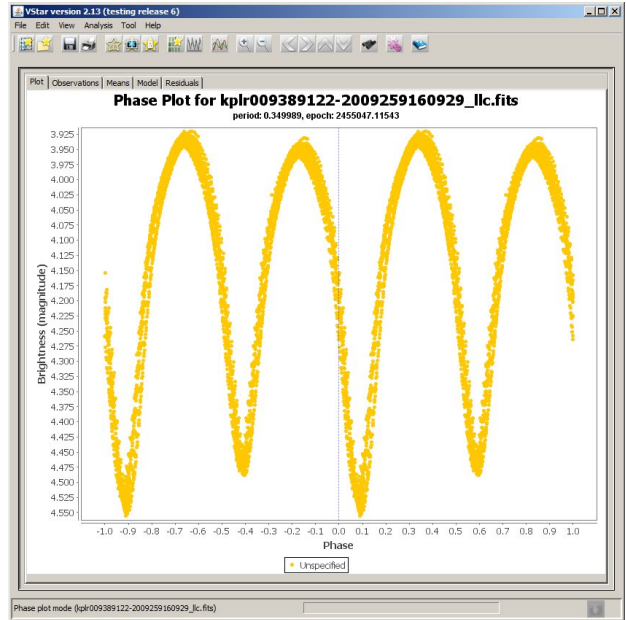


Figure 16. Initial Folded Lightcurve for kplr009389122 Using $P = 0.3499891$ d (Right)

This brings me to the final point of this article; why bother investigating a variable star with regular period(s) that have already been characterized in the literature? What may not be apparent to some readers is that the seemingly regular periodicity of many variable systems are subject to intrinsic and extrinsic influences which can perturb the exact timing of the orbital period or pulsation interval. Specifically in the case of eclipsing binary stars, the gravitational influence of an unseen companion, mass exchange between closely orbiting pairs, or star spot cycles can individually or collectively conspire to modify the orbital period or light curve shape within a relatively short time span. When the light curve data thus far collected for kplr009389122 are examined on a quarterly basis not only is it very obvious that there are far more than just subtle differences amongst all quarterly datasets but even within a single 90 day quarter, significant differences at maximum and minimum light can be observed. For example, a closer examination of the raw

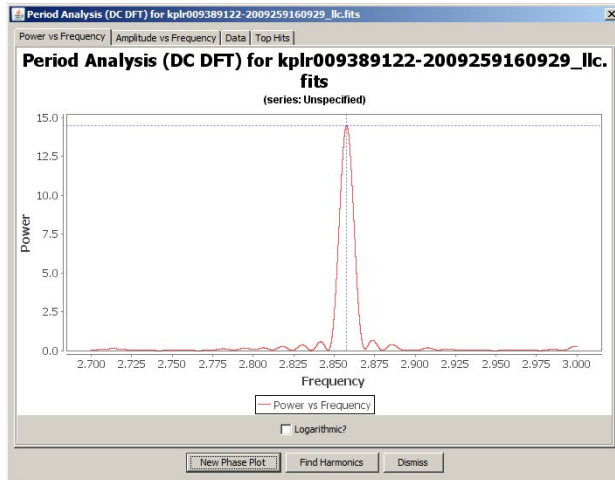


Figure 17. Higher Resolution (0.00001) DC DFT Period Analysis of kplr009389122-2009259160929 Between 2.7 and 3.0 d^{-1} (Above)

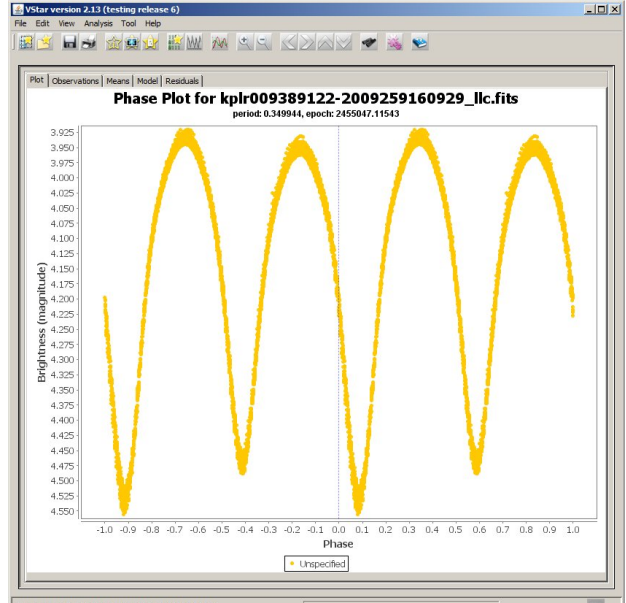


Figure 18. Phase Plot Establishing Refined Orbital Period (0.349944 d) for kplr009389122-2009259160929 (Right)

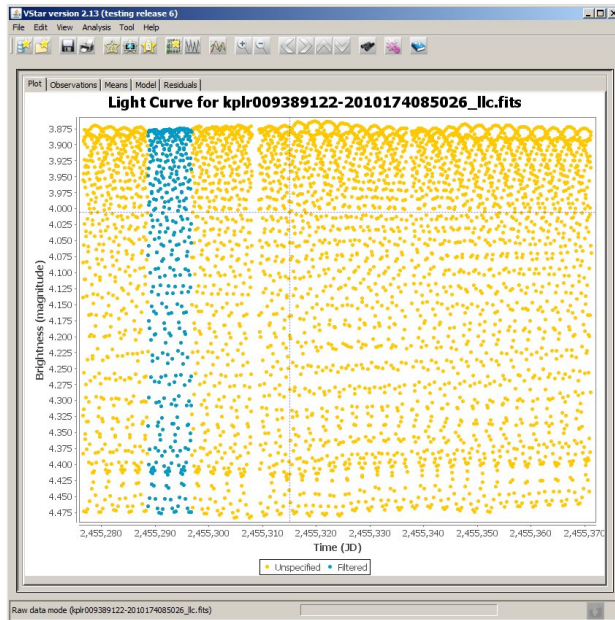


Figure 19. VStar View of Lightcurve Segment During Which Max I and Max II Appear Nearly Equal (Top Left).

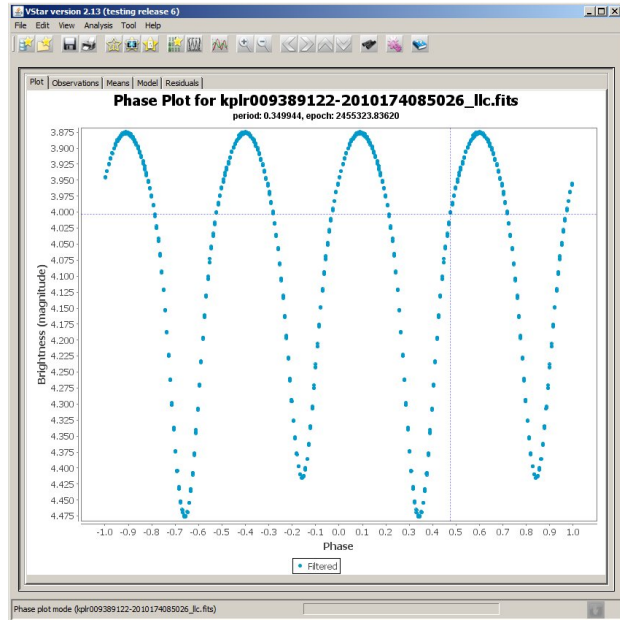


Figure 20. VStar Phase Plot During Period of Time When Maximum Light for kplr009389122 was Equal (Top Right).

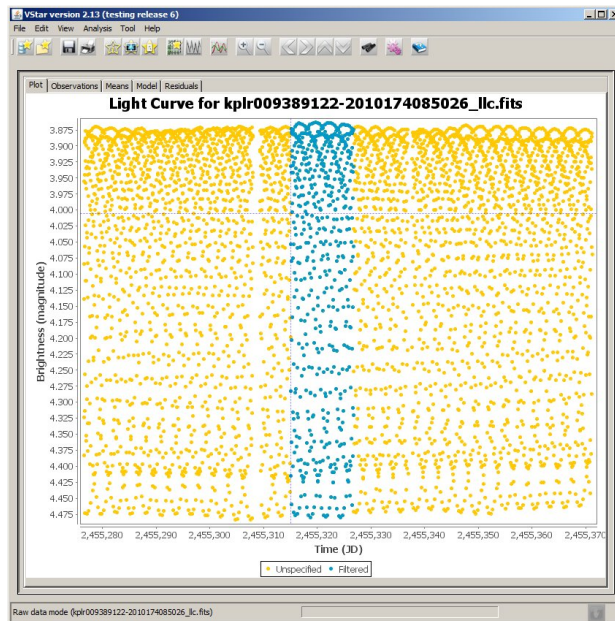


Figure 21. VStar View of Lightcurve Segment in Which Maximum Light is Not Equal (Bottom Left).

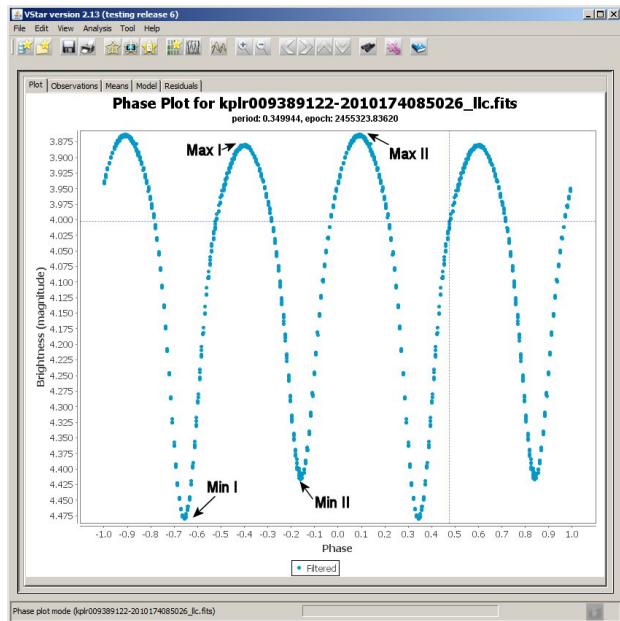


Figure 22. VStar Phase Plot During Period of Time for kplr00938912 when Max I < Max II (Bottom Right).

unfolded light curve from the 5th Quarter reveals that maximum light is oscillating with two crossover epochs centered circa BJD 2455292.5 and BJD 2455339.5 (Figure 19). In both cases $Max\ I \approx Max\ II$ as can be seen from a folded lightcurve (Figure 20) produced using only the highlighted subset of BJD vs flux. This is in significant contrast to another time segment (Figure 21) where folded light curves clearly show that $Max\ I \neq Max\ II$ (Figure 22); this type of asymmetry at maximum light is commonly called the O’Connell effect (Wilsey and Beaky 2009). In late type contact

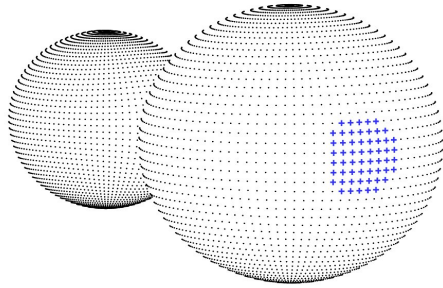


Figure 23. 3-D Model of W UMa Binary With Cool Starspot Positioned to Potentially Lower the Value of Min II (Top Left).

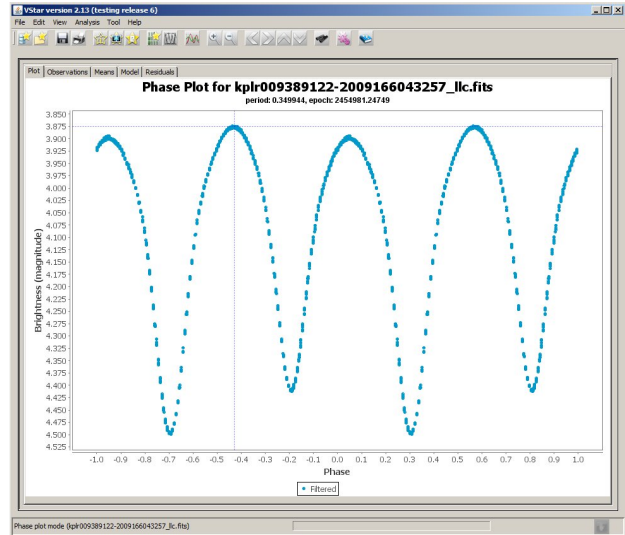


Figure 24. VStar Phase Plot During Period of Time for kplr00938912 When Max I > Max II (Top Right).

systems this phenomenon is often attributed to cool starspots or hot impacts from mass-transferring gas streams. These effects can be simulated using applications like Binary Maker 3, WDWint, or PHOEBE, all of which are based on the Wilson-Devinney code for Roche-type modeling.

Before tackling the simulation of lightcurves using Roche-type modeling there are a few other details that need to be addressed. By convention with eclipsing binary systems, the deepest minimum (Min I) generally occurs when the cooler secondary transits or occults the more massive and brighter primary constituent. In W UMa-type overcontact systems, the difference in T_{eff} between the primary and secondary is relatively quite small (<200 K). Given these modest differences, there are situations like that described for RT LMi (UnderOak Observer Issue 2) in which the deepest minimum occurs when the secondary is eclipsed (Min II). The combined effect of a large cool starspot on the primary star directly facing the viewer (Figure 23) while crossing the light path coming from the secondary may be enough to drive Min II to a fainter value than Min I. Starting with the linear ephemeris (Min I = BJD 2,454,964.90797 + 0.349950 E) for kplr009389122 (Prša et al 2011), one can quickly determine whether the deepest minimum at any epoch (E) is a primary or secondary. For example in Figure 12 the deepest minimum is observed at BJD 2455031.04500 while another less faint minimum appears at BJD 2455031.22891. According to the linear ephemeris the deepest minimum (Min I) appears 189 cycles after BJD₀, and the less faint minimum (Min II) appears as expected mid-way between cycles 189 and 190:

$$\begin{aligned} (2455031.04500 - 2,454,964.90797) / 0.349950 &= 189.0 \\ (2455031.22891 - 2,454,964.90797) / 0.349950 &= 189.5 \end{aligned}$$

This pattern is consistently observed throughout all the light curve data available to this point and suggests that there are no surprises regarding the true identity of Min I and Min II.

Aside from the example shown in Figure 19, there are two other separate blocks of time within the first five quarters during which Max I and Max II are very nearly equal. These are important periods of time when perhaps kplr009389122 is least perturbed by whatever phenomena is responsible for the O’Connell effect. It follows that the associated light curves might serve as a reference or anchor for any change to the system. Building further on this possibility, an examination of the folded light curves associated with symmetrical maximum light reveals that the brightness difference between maximum light and each of the two minima is fairly constant (Table 1). This being the case, another important behavior of this binary system may be proposed from a typical kplr009328122 light curve when Max I ≠ Max II. One example from the 5th quarter which was previously shown (Figure 22) illustrates that the brightness change between Min I and Max I is similar (0.599 vs 0.600) to the reference light curves. In contrast, the difference between Min II and Max II (0.554 vs 0.538) is greater than that observed when Max I = Max II.

Kplr009389122-	Quarter	BJD	Min I – Max	Min II – Max	Min I – Min II
2009350155506	3	2455101.17191 - 2455107.9965	0.600	0.535	0.065
2010078095331	4	2455238.85045 - 2455247.35096	0.601	0.539	0.060
2010174085026	5	2455288.17843 - 2455293.75699	0.600	0.540	0.060
Mean =			0.600	0.538	0.062

Table 1. Min I, Min II and Maximum Light Differences for kplr009389122 During Periods of Time in Which Max I = Max II

Hypothetically, if this system is undergoing active mass transfer then one possible explanation for this light curve morphology is the presence of a hot spot on one of the stars which contributes to the increased brightness of the binary system during second quadrature (Max II). It should be noted that this is entirely speculative in the absence of other supporting evidence such as that which might be obtained spectroscopically or by construction of an O-C diagram which can help piece together a model to describe the short-term and secular changes in eclipsing binary systems. Briefly (see UnderOak Observer Issue 1 for O-C Method Primer) a parabolic relationship between the observed vs calculated times-of-minima would suggest that the orbital period is changing linearly with time due to mass transfer or loss of angular momentum. In contrast to the previous example where Max II > Max I, another folded light curve (Figure 24) produced from kplr009389122-2009166043257 between BJD 2454964.5119 and BJD 2454977.9985 reveals that Max I was brighter than Max II thus illustrating the dynamical changes that eclipsing binaries can experience within a relatively short period of time. Arguably, a photometrist’s work is never completed on many variable star systems.

In closing, this first installment of “Mining the Kepler Database” is intended as an introduction to the vast amount of variable star data which is publically available from the Kepler Mission. Although this article was largely focused on the preliminary analysis of light curves from eclipsing binary systems, these variable types represent less than 2% of the total number of stars captured in the Kepler field. Based upon personally screening more than 20,000 Kepler light curves, if you are more interested in pulsating stars, then there is a much larger selection of these variable targets. “Mining the Kepler Database – Part II”, which is scheduled to appear in a future issue of the “UnderOak Observer”, will take a closer look at an O-C diagram produced by kplr009389122 (or potentially others) to see whether its light curve behavior can be synthesized using additional period analysis and Roche lobe modeling.

References

1. Prša, A., Batalha, N., Slawson, R.W., et al 2011, AJ, 141, 83.
2. Wilsey, N.J. and Beaky, M.M. 2009, SAS Proceedings, 107.
3. Templeton, M. 2004, JAAVSO, 32, 41.

Caveats:
 The "UnderOak Observer" is published advertisement free using Scribus (v1.3.3.14). Its intent is both entertainment and informational. Every reasonable effort is made to verify facts and avoid personal bias, however, the reader bears full responsibility for actually believing what I have written.

Cover Page Art:
 The Rosette Nebula (Caldwell 49) in Monoceros. Color was rendered using Registar after synthesizing green from red and blue images downloaded with the DSS Plate Finder (http://archive.stsci.edu/cgi-bin/dss_plate_finder).

Editor: Kevin B. Alton
 Writer: Kevin B. Alton

Public Access:
 Free access to any light curve data associated with research published in the UO can be obtained by request (mail@underoakobservatory.com)



Losmandy G11 Tune-up: Anatomy of an Ovision Worm-Gear Upgrade

The Losmandy G-11 is a remarkably robust German-equatorial-mount, but after suffering through four continuous years of use in my backyard observatory where the inside temperatures can range from 115°F in the summer to -5°F in the winter, it was time to consider a tune-up. An analysis of the mount performance in November 2010 using PHD Guiding (<http://www.stark-labs.com/phdguiding.html>) and PECPrep (<http://eq-mod.sourceforge.net/pecprep/index.html>) had revealed periodic error values fairly typical for an unmodified G-11 (Figure 1). Unguided peak-to-peak swings averaged ± 10.35 arcsec which interestingly appears to have a significant long period (2654.4 sec) component (Figure 2) that is an 11-fold multiple of the worm gear periodic error which occurs every 239.4 sec (Figure 3). The notorious G-11 resonance which appears every 76.2 sec as the ball passes the outer race of the worm bearing can be seen in Figure 4. Nearby, additional data filtering shows a small contribution from the third harmonic (79.8 sec) of the worm gear periodic error (Figure 5). The fast Fourier frequency spectrum displayed in Figure 6 provides a relative sense of magnitude associated with each periodic error component.

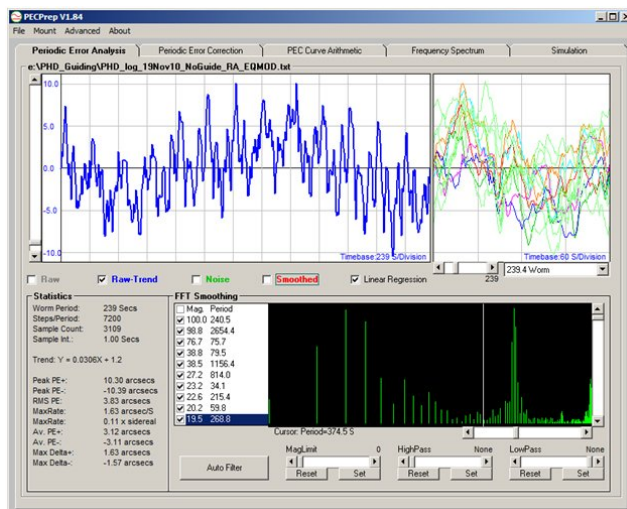


Figure 1. Periodic Error Analysis (PECPrep) showing Peak-to-Peak Variation in RA over 13 Worm Gear Cycles

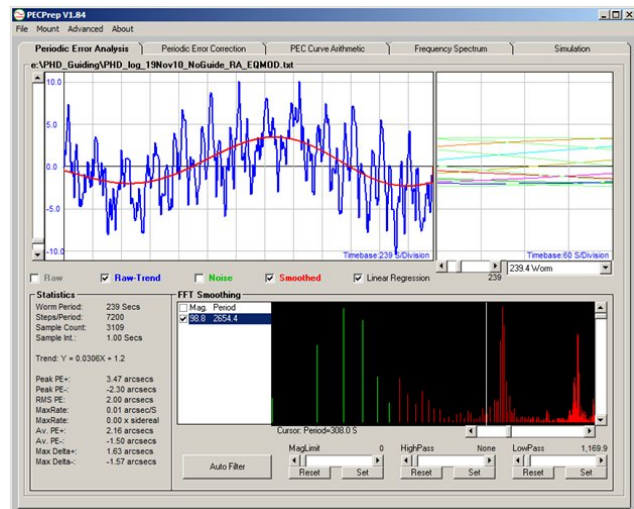


Figure 2. Periodic Error Analysis Showing Longest Component (2654.4 sec) Superimposed (red) onto Total Peak-to-Peak Variation

Table 1 Heads-up Comparison of Losmandy G-11 Performance Before and After Installation of Ovison NS Worm Gear Kit

Periodic Error	Unmodified G-11		Ovison Modified G-11	
	Unguided	Guided	Unguided	Guided
Peak (+) arcsecs	+10.3	+2.50	+3.94	+2.11
Peak (-) arcsecs	-10.39	-1.90	-4.32	-1.37
RMS arcsecs	3.83	0.71	1.53	0.45
MaxRate arcsec/S	1.63	2.12	1.21	2.31
MaxRate x sidereal	0.11	0.14	0.08	0.15
Avg (+) arcsecs	+3.12	+0.62	+1.16	+0.37
Avg (-) arcsecs	-3.11	-0.53	-1.3	-0.35
Max Delta (+) arcsecs	+1.63	+2.12	+0.96	+2.31
Max Delta (-) arcsecs	-1.57	-1.96	-1.21	-1.56

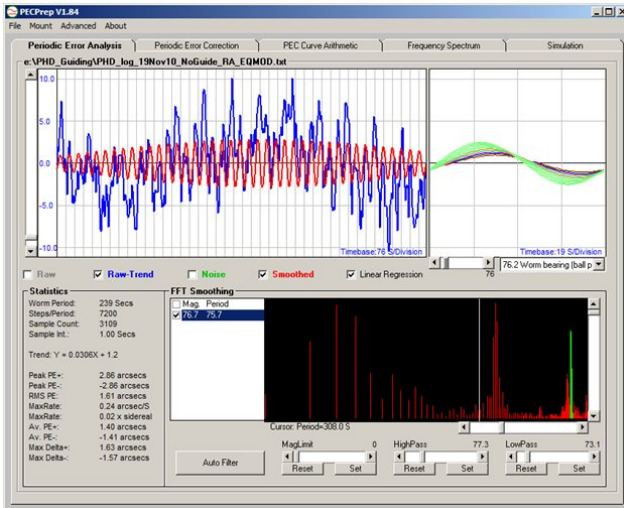
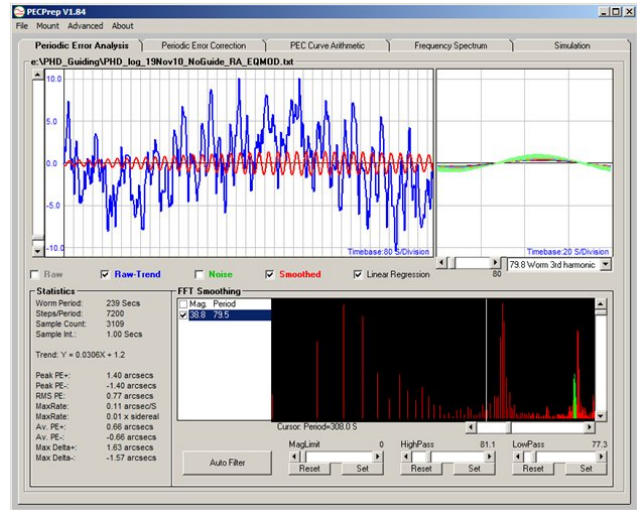
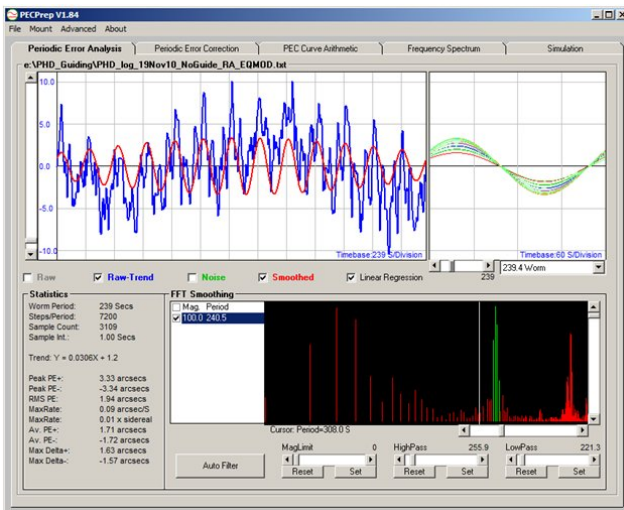


Figure 3 (Upper Left).
Periodic Error Analysis Showing Worm Gear Component (239.4 sec) Superimposed (red) onto Total Peak-to-Peak Variation with Unguided Stock G11

Figure 4 (Upper Right).
Periodic Error Analysis Showing Worm Gear Thrust Component (76.2 sec) Superimposed (red) onto Total Peak-to-Peak Variation with Unguided Stock G11

Figure 5 (Bottom Left).
Periodic Error Analysis Showing Worm Gear Third Harmonic (79.8 sec) Superimposed (red) onto Total Peak-to-Peak Variation with Unguided Stock G11

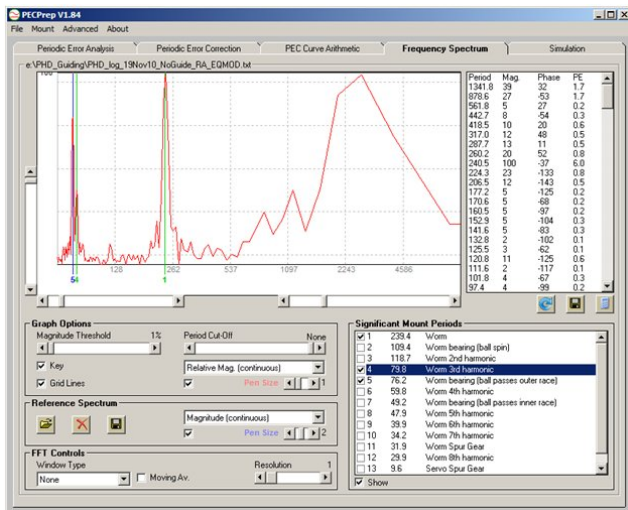


Figure 6 (Upper Left).

FFT spectrum showing relative contribution of important periodic error components with Unguided Stock G11

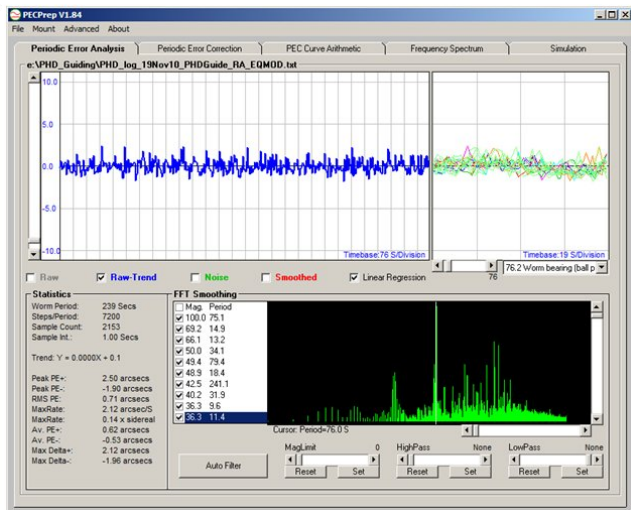


Figure 7 (Upper Right).

Periodic Error Analysis Showing Total Peak-to-Peak Variation with Guided Stock G11

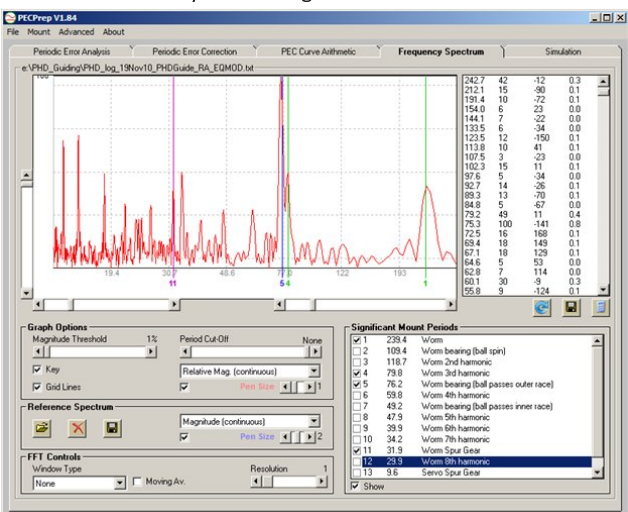


Figure 8 (Center Left).

FFT Spectrum Showing Relative Contribution of Important Periodic Error Components with Guided Stock G11

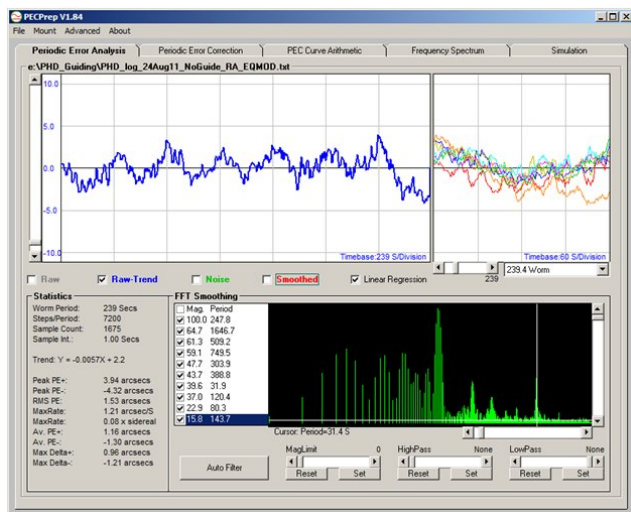


Figure 9 (Center Right)

Periodic Error Analysis Showing Peak-to-Peak Variation in RA with Unguided Ovison Modified G11

As can be seen in Figure 7 and Table 1, guiding significantly attenuates the peak periodic error (+2.5 to 1.9 arcsec). While both the long period (2654.4 sec) and worm gear (239.4 sec) PE are effectively removed, inspection of the frequency spectrum (Figure 8) illustrates the difficulty in guiding on both the 76.2- and 79.8-sec periodic errors inherent to the RA gear-drive mechanism in the G-11. Further improvement

can only be realized with a new worm gear assembly which addresses this design flaw; the Ovison NS kit was selected based upon very positive feedback from within the amateur astronomy community. Since “she who must be obeyed” was not receptive to the idea of buying either a Paramount ME (\$8995) or Astro-Physics mach1GTO (\$6350), the total cost to potentially achieve similar PE specs (7 arcsec



Figure 10 (Upper Left). Analysis Showing Composite Worm Gear (239.4 and 119.7 sec) and Worm Gear Thrust (76.2 sec) Periodic Error Superimposed (red) onto Total Peak-to-Peak Variation with Unguided Ovision Modified G11

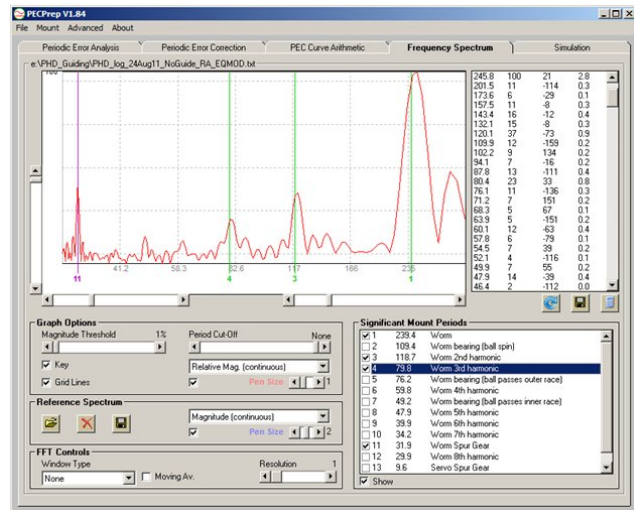


Figure 11 (Upper Right). FFT Spectrum Showing Relative Contribution of Important Periodic Error Components with Unguided Ovision Modified G11

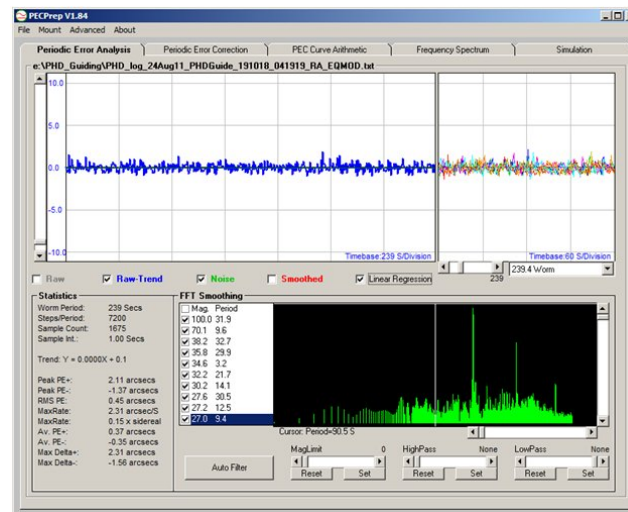


Figure 12 (Center Left). Periodic Error Analysis Showing Total Peak-to-Peak Variation with Guided Ovision Modified G11

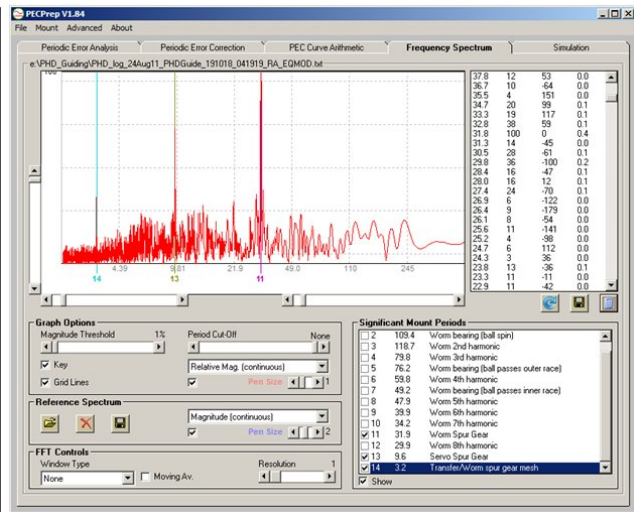


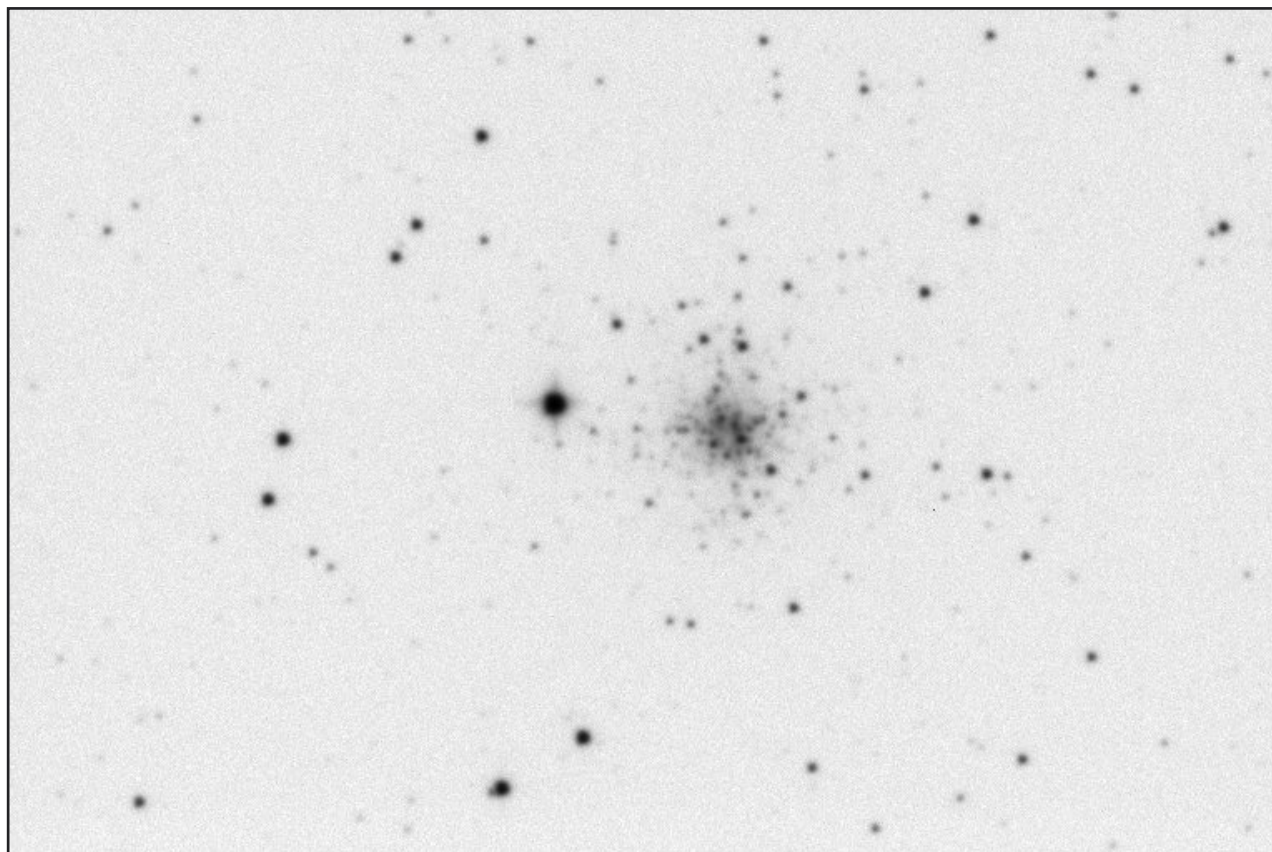
Figure 13 (Center Right). FFT Spectrum Showing Relative Contribution of Important Periodic Error Components with Guided Ovision Modified G11

peak-to-peak unguided) was by comparison a bargain. Still, factoring in the worm gear purchase price (\$499), international shipping (\$30), customs duty (\$147) and installation (\$65) which also included a base tune (\$375) by the good folks at Astrotroniks (<http://www.astrotroniks.com/store/>), the total

amount (\$1116) was not inconsequential. Fortunately, this proved to be a good investment given the overall improvement in mount performance. Immediately obvious in the unguided Ovision PE profile (Figure 9) was an apparent attenuation of the long period periodic error previously observed with

the stock worm gear (Figure 1). Total peak-to-peak (8.26 arcsec) had similarly decreased 2.5-fold and was largely associated with periodicity from the worm gear and its second harmonic. The only other meaningful periodic error was attributed to the worm spur gear (31.9 sec) which largely contributed to the toothy look of the sinusoidal-like waveform (Figure 10). Guiding very effectively removed all evidence of the worm gear periodic error and its even harmonics (Figure 11), however, noise associated with the spur gear at 31.9, 9.6, and 3.2 sec was still fairly obvious as discrete peaks in the FFT spectrum (Figure 12). Arguably, this remaining source of periodic error is what keeps the Ovision modified Losmandy G-11 from being a world-class performer on par with the Paramount ME and Astro-Physics mach1GTO mounts. Nonetheless, my

goal of achieving guided sub 4 arcsec peak-to-peak performance has been realized with a modest investment in an already very good German equatorial mount. A typical photometric session lasting from 3 to 5 hours capturing hundreds of 1 to 1.5 minute exposures rarely produces any out-of-round stars unless the guide camera loses contact with the guide star due to cloud cover. Now, to be equally successful in finding a way to eliminate differential flexure with my side-by-side saddle mounted scopes, would make me one happy camper.



Guided, but unregistered stacked (1 x 11 min) image of the globular cluster NGC 6934 taken with an ST402ME (I_C band) and VC200L catadioptric telescope after Modifying Losmandy G11 with an Ovision worm gear. Compared to individual images, star shape (elongation <0.02 as determined with AIP4Win) in stacked image is equally well behaved.

Research Article

A cursory look at the potential use of HyperStar based optics for the photometric measurement of variable stars or asteroids

My curiosity was piqued by recent discussion on a popular amateur astronomy forum regarding the suitability of Fastar (aka HyperStar; <http://www.hyperstarimaging.com/evolution.php>) optics for the photometric evaluation of variable stars or asteroids. A lot of opinions were offered both pro and con regarding the suitability of very fast optics but no one provided any evidence from hands-on experience. Rather than speculating whether robust photometry is possible with HyperStar f/1.95 optics,

the standard photometric imaging system (8" catadioptric @ f/6.3 – ST402ME ccd) at UnderOak Observatory was replaced with a HyperStar 3 - NexStar 8 – SXVF-8MC combination which had only been used in the past for conventional astrophotography. Although the SXVF-8MC is a one-shot color camera (Sony ICX406AQ SuperHAD CCD), when binned (2x2) the resulting image is effectively monochromatic and does not need to be de-Bayered. The field-of-view (FOV) produced with this optical

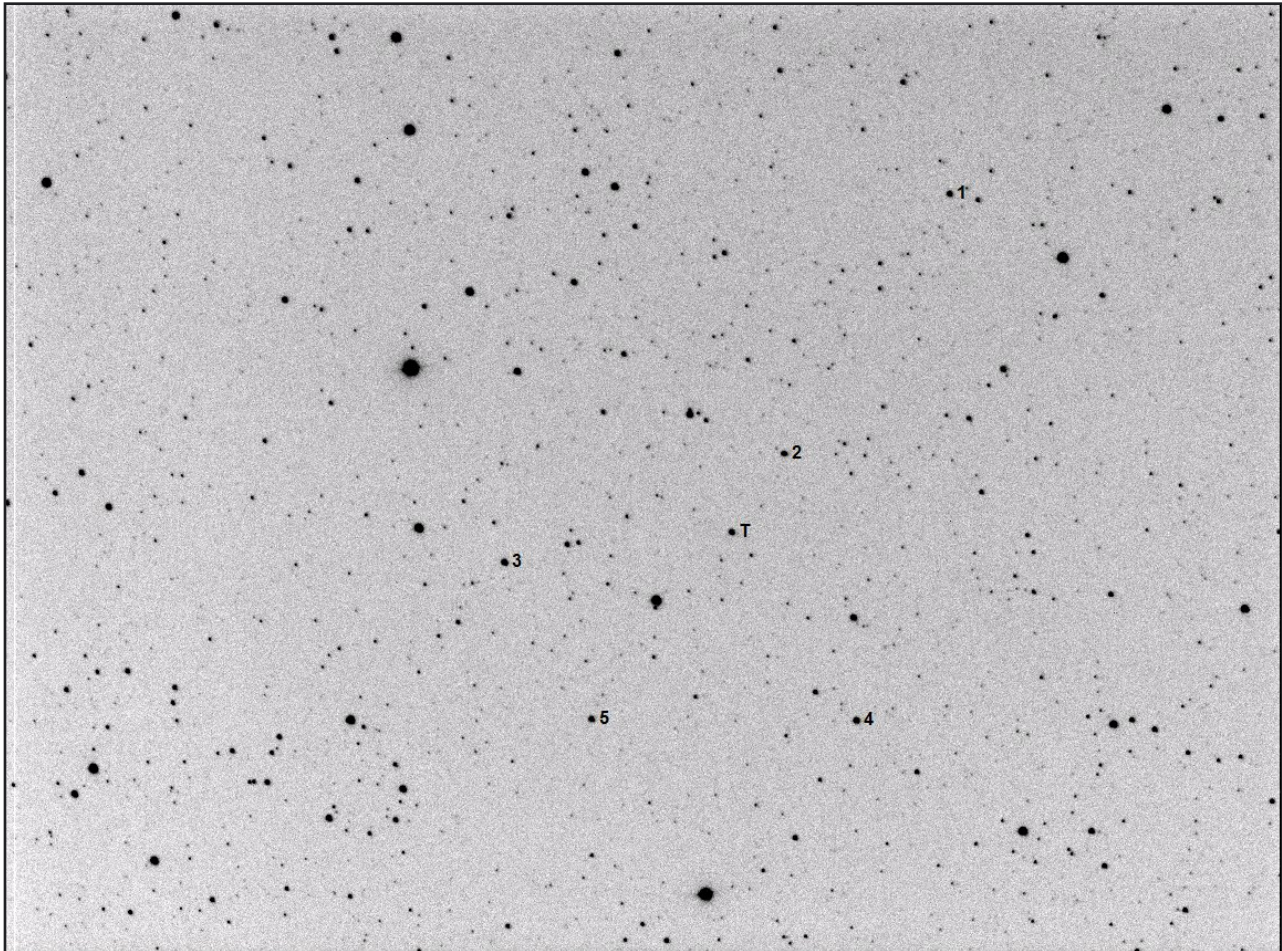


Figure 1. Image (40 sec) taken of 39 Laetitia (T) and Comparison Stars (1-5) With a HyperStar 3 Equipped NexStar 8 SCT. FOV Center is Located at RA = 07^h 01^m 41^s and Dec = 15° 12' 23".

train is 47×64 arcmin with an image scale of 3.3 arcsec/pix. Previous experience had shown that this setup is very sensitive to collimation. This is the reason why the HyperStar 3 optics is dedicated to a single OTA at UnderOak, which happens to be a deforked NexStar 8 GPS. The star field shown in Figure 1 was analyzed by CCDInspector which importantly revealed that focus can be uniformly maintained to the edge of the image with precise collimation (Figure 2).

Experimentally, two different targets were chosen, both of which were in the constellation Gemini. The first was GW Gem (3Mar2012 and 5Mar2012), a semi-detached eclipsing binary (period = 0.65944 d) that

ranges in Vmag from 10.5 to 11.4 and the second was 39 Laetitia, a main-belt minor planet now (6Mar2012) wandering through the “Great Twins”. Although the skies were somewhat hazy (as is often the case in NJ on a “clear” night) and the moon was annoyingly near full in the same region of the night sky, there was actually an advantage with this scenario. The extent of vignetting with such fast optics was likely to be the best possible test of what can be corrected with flats. One of the criticisms voiced about HyperStar optics was the potential for field curvature which could adversely affect astrometric measurements or the ability to plate solve. This did not prove to be the case with the HyperStar 3 – SXVF-8MC system. Plate solutions were easily achieved (residuals <0.6 arcsec)

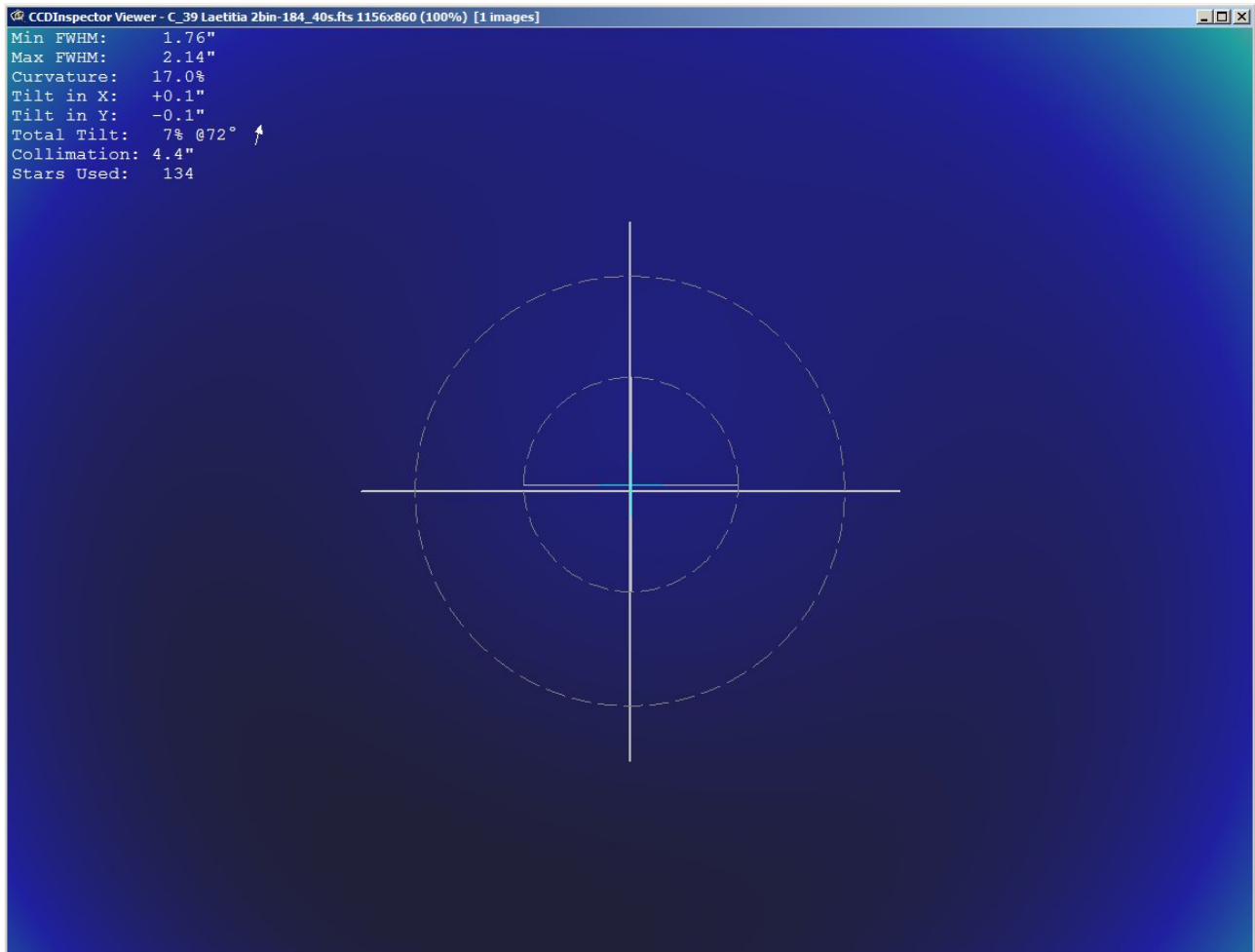


Figure 2. CCD Inspector Analysis of a Single 40 sec Exposure of Starfield Around 39 Laetitia Showing Fairly Uniform Good Focus Across the Entire FOV

with the astrometric database employed by MPO Canopus as well as that used in PinPoint (MaxIm DL 5). A 40-sec exposure time provided a good compromise between sensitivity, linearity, and vignette effects from sub-par seeing and transparency. Raw images were reduced and registered using AIP4Win and lightcurves produced using MPO Canopus. Fortunately, vignetting was largely attenuated with simple observatory dome flats using a median master produced from 10×4 sec images. As can be seen in Figure 3, the primary minima predicted for GW Gem occurred during both observing sessions which (as expected) were virtually identical in magnitude at minimum light (Min I). Since no filter was used, the magnitude (y-axis) is an estimated Vmag value but nonetheless consistent with literature values (Broglia & Conconi 1981) for this binary system. Based on the s/n associated with stars dimmer than GW Gem, there is a reasonable likelihood that quantitative photometry (± 0.05 mag) with this system can reach down to at least Vmag 13.

As of 02:45:00 UTC on 07March2012, the magnitude of 39 Laetitia was estimated at 11.12 using the “Asteroid Browser” in MPO Canopus. A partial lightcurve (Figure 4) was obtained which covered about 68% of the synodic period (5.138 h) for this minor planet. Although the magnitude (V) expressed on the y-axis was estimated from 5 comparison stars with similar brightness in the same FOV, flux change relative to fixed comparators is all that is needed to calculate the synodic period of asteroids. It should be noted that thus far the lightcurve amplitude (~ 0.22 mag) is within the values reported in the literature for 39 Laetitia (Kaasalainen et al 2002).

Summary

Although not ideally suited for high precision photometry, HyperStar 3 optics coupled with an appropriate ccd camera and filter(s) is capable of producing good quality lightcurves from variable stars and minor planets. Special care must be taken to precisely collimate and properly focus HyperStar optics to obtain the best results. As with any quantitative analysis, it is important to operate within the linear range of the detector. Certainly neither the target nor any comparison object can be saturated; how close to saturation linearity extends is highly dependent on the ccd. In the real world of sub-par

photometric conditions where most amateur astronomers live, vignetting will be a challenge to correct with such fast optics, but within limits, not impossible. The large FOV can be an advantage if you plan to screen for variable or moving objects in a broader area of the sky than that typically covered by purpose-designed systems set up for precise photometry. If you endeavor to track a minor planet and generate light curves, it may be possible to use the same comparison stars over multiple days if the starting point on the image is strategically positioned on a diagonal to allow maximum movement across the FOV. Keeping the same comparison stars should improve the overall quality of the data. For example from its ephemeris starting on 07Mar2012, 39 Laetitia would take nearly 10 days to traverse the FOV covered by the HyperStar 3 – SXVF-8MC equipment described above.

Hopefully the positive results from this study will encourage those who might be interested in photometric research but do not wish to dismantle their HyperStar setup. Moreover, despite the many opinions to the contrary, there is every reasonable expectation that similar success can also be obtained with other CCD detectors compatible with HyperStar optics.

References

- Broglia, P. and Conconi, P. 1981, “Photometry and Elements of GW Geminorum”, *Astro. Astrophys. Suppl. Series*, 46, 185.
 Kaasalainen, M., Torppa, J. and Piironen, J. 2002, “Models of Twenty Asteroids from Photometric Data”, *Icarus*, 159, 369.



HyperStar 3 - 8" Lens Assembly Which Replaces Secondary Mirror in Celestron SCT

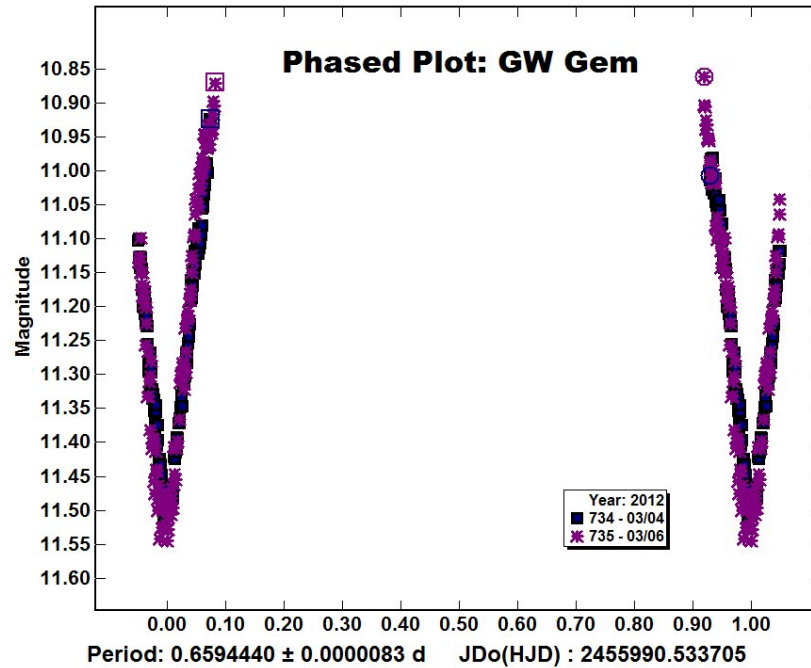


Figure 3. Phased Plot from Lightcurve Data Collected from GW Gem Using a Hyperstar 3 Equipped NexStar 8

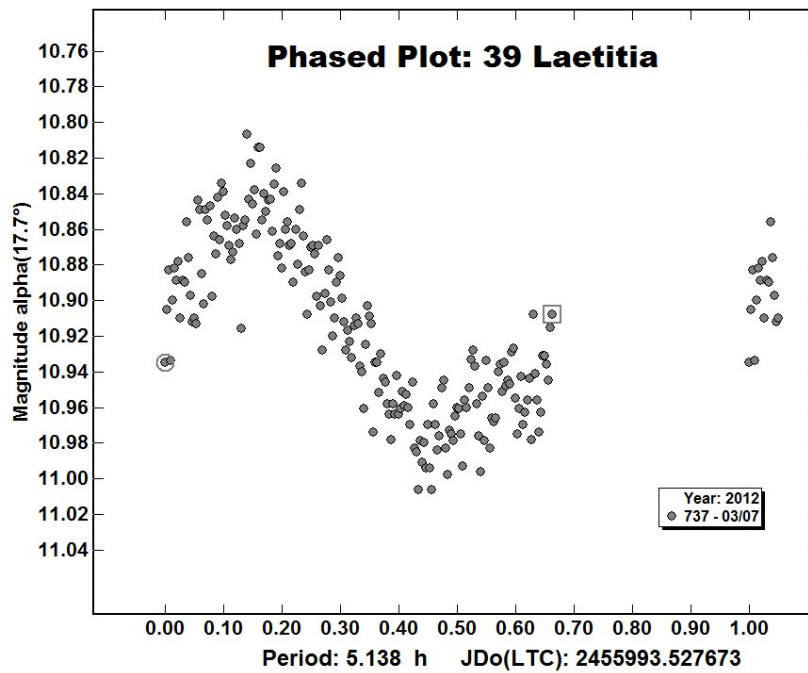


Figure 4. Phased Plot from Lightcurve Data Collected from 39 Laetitia Using a Hyperstar 3 Equipped NexStar 8